Time domain full waveform inversion algorithm using common scatter point gathers

Hassan Khaniani, John C. Bancroft and Gary F. Margrave

ABSTRACT

Full Waveform Inversion (FWI) on acoustic seismic data is based on data prediction using an updated velocity model. The key concept in the updating process is calculating the gradient of a miss-fit function, which is the difference between actual data and the predicted data. In each step, the gradient function, in either the time or frequency domain, is estimated by depth migration algorithms.

We have developed a fast full waveform inversion scheme that is based on the Pre-Stack Time Migration (PSTM). We use the forward Kirchhoff operator for prediction of shot records from the reflectivity function. Then we derive the adjoint operator for velocity perturbation using shot perturbation. We obtained a similar solution of the inverse problem by Prestack Kirchhoff Time Migration (PSTM) and crosscorelation with the source wavelet.

The methodology is fast compared to any PSDM techniques in forward and inverse iterations; however, our forward operator is assumed to be linear with negligible lateral velocity change. Therefore, since we are doing time migration, we are limited to models without complex structures.

INTRODUCTION

For several years accurate seismic imaging has major challenges for geophysical data processing from the accuracy and the computation point of view. The accuracy of the image depends on the application of the wave equations on the recorded data and the input parameters from the medium. Recently, seismic full waveform inversion (FWI) (Tarantola, 1984; Pratt et al., 1998; Pratt, 1999) has become an increasingly practical tool for estimating subsurface parameters (Ma, 2010).

Seismic waveform inversion is based on model-based fitting of waveform data (Symes, 2008). It is often formulated as to minimize the least-squares problem of reducing the energy in the difference between predicted and observed data, by updating the model on which the prediction is based.

To study the long history of FWI the reader is referred to Virieux and Operto (2009). The main obstacles that have prevented its common application in exploration seismology are its computational costs and the need for starting model update (Ma, 2010). FWI requires a huge amount of seismic data prediction and gradient calculation.

Various efforts from different perspectives have been expended to reduce the computational costs associated with gradient calculation and data prediction. For example Sirgue and Pratt (2004) and Operto et. al., (2007) limit the number of frequencies in updating model. Vigh and Starr (2006) used plane-wave method for 3D problems and

Margrave et. al., (2010) used Phase Shift Plus Interpolation (PSPI) one way wave equation for gradient calculations.

In this work we start with the use the forward Kirchhoff operator for prediction of shot records from the reflectivity function (Schneider, 1978, Bleistein et. al., 2001). Then we derive the wavefield perturbation as a result of the velocity perturbation. This results to a similar solution of inverse problem as Prestack Kirchhoff Time Migration (PSTM) and crosscorelation with the source wavelet. This is similar to the result of Tarantola (1984) that showed classical PSDM migration and its forward modeling can be used in the inverse process.

The methodology is fast compared to any PSDM techniques in forward and inverse iterations; however, we have limitation in doing the method in the models with complex structures. This is because our forward operator is assumed to be linear with negligible lateral velocity change.

THE FORWARD PROBLEM

The Kirchhoff integral solutions to the wave equation are addresses by several outhors (e.g., Schneider (1978) and Bleistein et al., (2001)). In the general case where the velocity inside the Earth is arbitrary, the Double Square Root (DSR) equation serves as a starting point for total traveltime approximation for time migration that includes the time from the source to the scatter point plus the time from the scatter point to the receiver

$$t=\sqrt{\frac{\tau^2}{4}+\frac{(x+h)^2}{v^2}}+\sqrt{\frac{\tau^2}{4}+\frac{(x-h)^2}{v^2}}, \tag{1}$$

where the parameters τ is zero offset two-way travel time, h is the half source/receiver offset, x is the distance from source/receiver midpoint to lateral coordination of scatter point and v is the migration velocity. For simplicity equation (1) can be stated as single square root by

$$t=\sqrt{\tau^2+\frac{4h_e^{\,2}}{v^2}}, \tag{2}$$

where $h_e^2=x^2+h^2-\left(\frac{2xh}{vt}\right)^2$ is equivalent offset domain that collocate the sources and receivers in PSTM (Bancroft et al, 1998). In this approximation, assuming migration velocity to be close to RMS velocity (negligible lateral variation in velocity and limited offset) the shot record prestack volume $u(x,h,t)$ for a 2D problem can be obtained using Common Scatter Point (CSP) gathers $u(x,h_e,\tau)$

$$u(x,h,t)=\int Ku(x',h_e(x',h),\tau=\sqrt{t^2-\frac{4h_e^{\,2}}{v^2}})d\tau dh_e dx', \tag{3}$$

and the adjoint operator for migration is

$$u(x,h_e,\tau)=\int K^{*}\frac{\partial}{\partial\tau}u(x',h,t=\sqrt{\tau^2+\frac{4h_e^{\,2}}{v^2}})dtdhdx'. \tag{4}$$

The parameter K is the true amplitude term (Sun and Gajewski, 1997, Bleistein, 2001) and K^{*} is its adjoint operator. Equations (3) sprays the energy of CSP gathers along with DSR equations to model the shot records. The migration operator is diffractions stack integral in equation (4) that sums the distributed energy and locate it on stacked section $u(x,h_e=0,\tau)$.

If the lateral velocity variation is negligible, we can approximate the $u(x,\tau)=u(x,h_e=0,\tau)$ by convolution of reflectivity function with source wavelet $s(\tau)$ using

$$u(x,\tau)=-\frac{1}{4}\frac{\partial}{\partial\tau}L\,\mathrm{n}\left(\frac{1}{v(x,\tau)}\right)^2 * s(\tau), \tag{5}$$

where the density is assumed to be constant. Now the scattered field due to a perturbation to velocity field (i.e., $\delta u(u,t)$ due to $v+\delta v$) can be estimated by linearization of the velocity perturbation and the wavefield perturbation. We obtain from (5)

$$u(x,\tau)+\delta u(x,\tau)=-\frac{1}{4}\frac{\partial}{\partial\tau}Ln\left(\frac{1}{v(x,\tau)+\delta v(x,\tau)}\right)^2 * s(\tau), \tag{6}$$

and using Taylor expansion we have

$$\frac{1}{(v+\delta v)^2}=\frac{1}{v^2(x,\tau)}-\frac{2\delta v}{v^3(x,\tau)}+o(\delta v)^2, \tag{7}$$

where $o(\delta v)^2$ is higher order of approximation in the Taylor expansion. We obtain

$$u(x,\tau)+\delta u(x,\tau)=-\frac{1}{4}\frac{\partial}{\partial\tau}\left(\frac{1}{v^2(x,\tau)}-\frac{2\delta v(x,\tau)}{v^3(x,\tau)}-1\right) * s(\tau), \tag{8}$$

where the logarithmic function has been linearized by Taylor series expansion if $0<\frac{1}{v^2}-\frac{2\delta v}{v^3}<2$. Using similar Taylor expansion of equation (5) for $u(x,\tau)$, from (8) we readily obtain

$$\delta u(x,\tau)=\frac{\delta v(x,\tau)}{2v^3(x,\tau)} * \dot{s}(\tau)+o(\delta v,\delta u)^2. \tag{9}$$

Here we used the linear property of derivative of convolution operator. Finally from (3) and (9) we have

$$\delta u(x,h,t)=\int K^{*}\left(\frac{\delta v(x,\tau=\sqrt{t^{2}-\frac{4h_{e}^{2}}{v^{2}}})}{2v^{3}(x,\tau)}*\dot{s}(\tau)\right)d\tau dh_{e}dx'. \tag{10}$$

Equation (10) describes the change of recorded shot record $\delta v(x,\tau)$ if the velocity field is perturbed by $\delta v(x,\tau)$.

THE INVERSE PROBLEM

Let us point out that (10) is similar to (10) of Tarantola (1984) and (6) of Cohen and Bleistein (1979). The main difference is that here we have $\delta v(x,\tau)$ which is function of time and not on depth (i.e., $\delta v(x,z)$). This follows that without the loss of generality, to estimate $\delta v(x,\tau)$, we can impose similar inversion algorithms that are used for inversion of $\delta v(x,z)$.

In this work the inverse process are posed as a steepest decent algorithm that minimizes the second norm of $\delta u(x,\tau)$ (if $\delta v(x,\tau)$ is small)

$$\min\phi=\frac{1}{2}\sum_{x_s,x}\left\|\delta u(x,t)\right\|_{2}^{2}. \tag{11}$$

From (10) the $\delta v(x,\tau)$ is obtained by

$$\delta v(x,\tau)=2v^{3}\int K^{*}\frac{\partial}{\partial\tau}\dot{s}(\tau)*\delta u(x',h,t=\sqrt{\tau^{2}+\frac{4h_{e}^{2}}{v^{2}}})dtdhdx'. \tag{12}$$

Using the convolution property $\int dt\left(f(t)*g(t)\right)h(t)=\int dtf(t)\left(g(t)*h(-t)\right)$ we finally obtain

$$\delta v(x,\tau)=\left[2v^{3}\int K^{*}\delta u(x,h,t=\sqrt{\tau^{2}+\frac{4h_{e}^{2}}{v^{2}}})\right]*\ddot{s}(-\tau)dtdhdx', \tag{13}$$

which implies that the theory needs migration and cross-correlation with source function. From the equations (10) and (13) we can iterate

$$v_{k+1}(x,\tau)=v_{k}(x,\tau)+\alpha_{k}\gamma_{k}(x,\tau), \tag{14}$$

where $\delta u(x,\tau)=\gamma(x,\tau)$ and $\delta v_{k}(x,\tau)=\alpha_{k}\gamma_{k}(x,\tau)$.

To study the kinematical difference of the algorithms using PSDM and PSTM, Figure 2 shows a simple velocity model in depth. We assumed the density is constant and as shown in Figure 2a the reflectivity occurs at z_1 from v_1 and v_2. Assuming amplitude corrected data, for starting model the velocity is constant v_1 as shown in Figure 2b. In Figure 2c the estimated gradient $\gamma(z)$ is $R_{1}\frac{v_{1}^{3}}{8}H(z=z_{1})$ (see e.g., Innanen, 2011).This shows that after the first iteration the updated velocity is exactly the true velocity (i.e., $v_2 = v_1 + \alpha H(z - z_1)$, $\alpha = \frac{8(v_1 + v_2)}{v_1^3}$). In Figure 3 the same model is plotted in time. The computed gradient function $\gamma(\tau)$ is $R_1 \frac{v_1^3}{8} H(\tau - \tau_1)$. Similar result can also be obtain in solving equation (13) that the coefficient $\frac{1}{8}$ is recovered by $2K^*$. For the true model in Figure 2a similar analysis are shown if the starting velocity be a step function at z_2 (Innanen, 2011). The gradient function is a boxcar as shown in Figure 3c. If we consider the τ as a pseudo z, the time domain gradient $\gamma(\tau)$ in Figure 4c will have similar shape to depth domain. The difference is for its stretching due to velocity depth to time conversion effects.

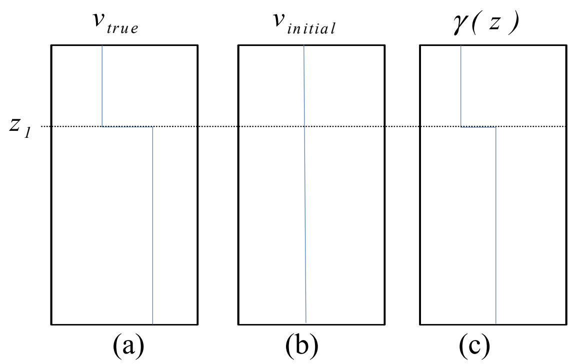

FIG. 1: Kinematics of FWI using depth migration. a) plot of velocity $v(z)$ versus depth z for model 1. b) The first iteration velocity in depth and c) The gradient of misfit function $\gamma(z)$ in the first iteration.

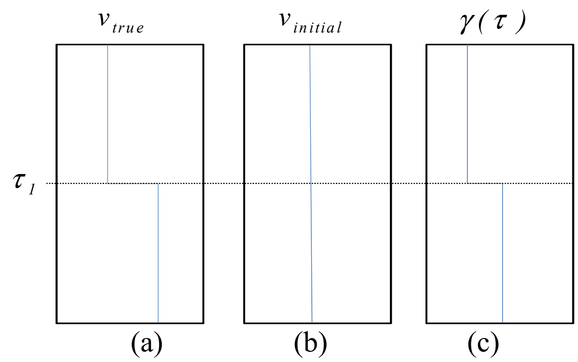

FIG. 2: Kinematics of FWI using time migration. a) plot of velocity $v(\tau)$ versus depth τ for model 1. b) The first iteration velocity in time and c) The gradient of misfit function $\gamma(\tau)$ in the first iteration.

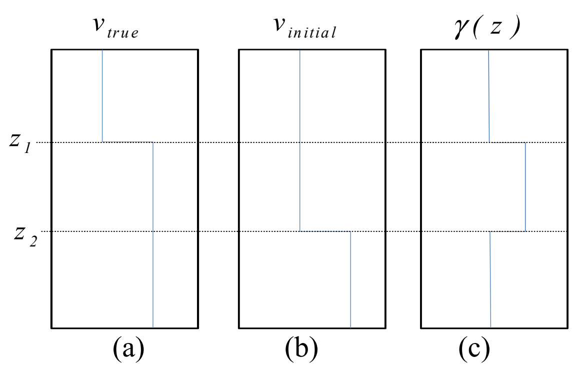

FIG. 3: Kinematics of FWI using depth migration. a) plot of velocity $v(z)$ versus depth z for model 2. b) The first iteration velocity in depth and c) The gradient of misfit function $\gamma(z)$ in the first iteration.

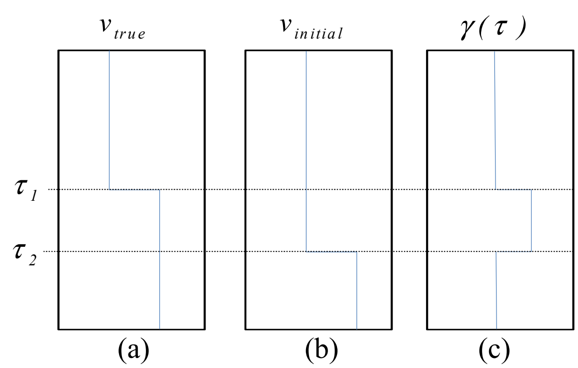

FIG. 4: Kinematics of FWI using time migration. a) plot of velocity $v(\tau)$ versus depth τ for model 2. b) The first iteration velocity in time and c) The gradient of misfit function $\gamma(\tau)$ in the first iteration.

The flowchart for FWI algorithm using PSTM is shown in Figure (5). At each frequency the first step is to convert $v(x,\tau)$ to RMS velocity $v_{rms}(x,\tau)$. The shot records are generated by Kirchhoff forward operator from the reflectivity function. The difference between recorded data and synthetic data $\delta u(x,t)$ computed for the current model. To calculate $\gamma(x,\tau)$ PSTM migrates the residual $\delta u(x,t)$ using (4) to compute $\delta u(x,\tau)$. Then the algorithm searches for step length α for the steepest descent and then computes the updated model using (14). Once the convergence is small enough the next frequency iteration are performed.

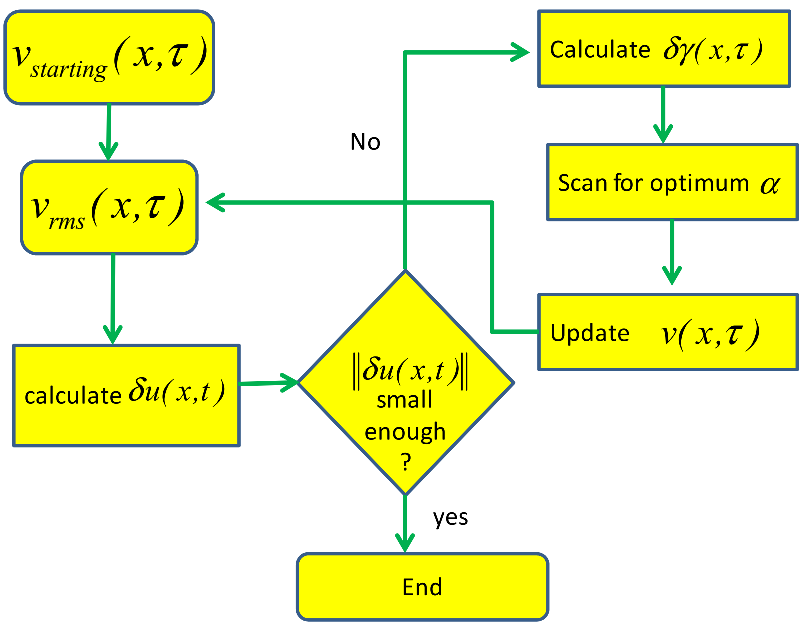

FIG. 5: Simplified algorithm for updating velocity using time migration FWI algorithm.

MARMOUSI NUMERICAL EXAMPLE

To perform a successful velocity update, we select the left part of Marmousi velocity model (Figure 6a). The small lateral variation of the velocity within the model ensures that the Kirchhoff forward operator for shot records has fair match with that from finite difference wave propagations techniques. Using depth to time conversion algorithm, the $v(x,z)$ converted to $v(x,\tau)$ and then 21 shots are recorded each with 201 receivers in split spread configuration. The first shot is at surface of $1250m$ lateral coordination and the last shot is at $2250m$. Wavelet is minimum phase and the dominant frequency changes from 5 Hz to 12 Hz depending on iterations. For the starting velocity the true model smoothed to $700m$ using Gaussian smoother (Figure 6c). The iteration starts with 5 Hz shots record to 12 Hz to update the velocity. At each iteration 9 values of α coefficient on normalized residual stack has been tested. Optimum α is found by the interpolation of the minimum norm of $\|\delta u(x,t)\|_2^2$. Figures 6d & 7 illustrate the success of the method. Figure 6d shows the updated velocity after 45 iterations which indicate we can invert the velocities of different layers. As shown in Figure 7 the updated velocity at 1800*m* of the model gives overall estimation of true model (see e.g., high velocity layer at 1.75s).

The trend of updated velocities at 1800*m* of the model for 45 iterations is shown in Figure 8. Figure 9 compares an updated shot record with the true shot record at 1800*m* that we have assumed multiple free data sets and only PP reflected wave type.

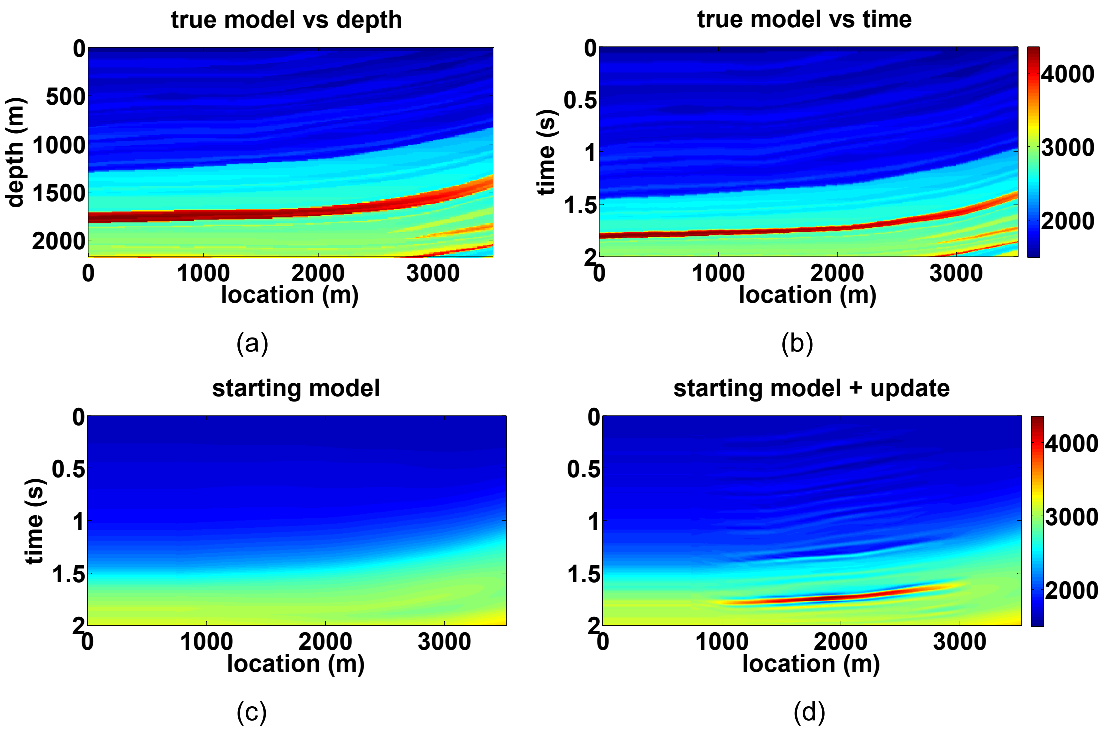

FIG. 6: FWI using PSTM for Marmousi model using 21 shots from 1250*m* to 2250*m*. a) True velocity vs depth b) True velocity vs time c) starting velocity d) The inverted velocity after 45 iterations.

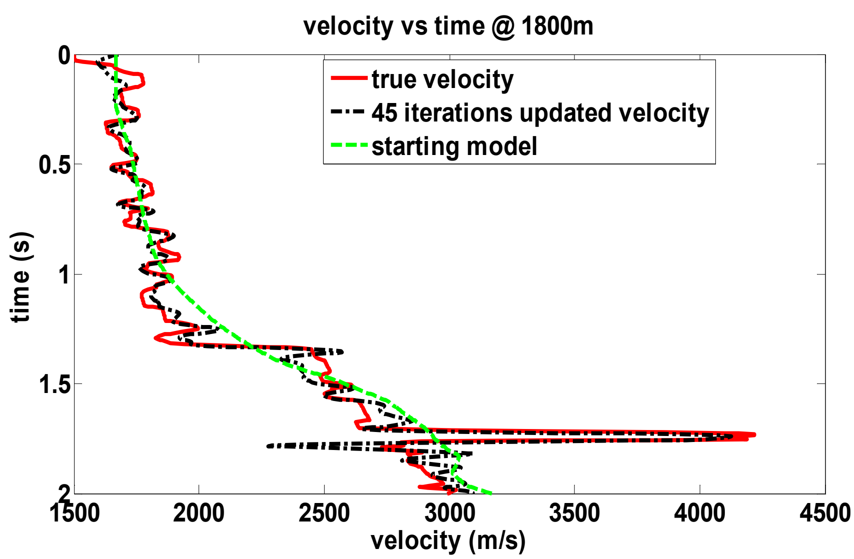

FIG. 7: Comparison between the true velocity model (solid red) the starting model (green dashed) and the FWI model (dashed dot black) using the PSTM strategy at 1800m lateral position.

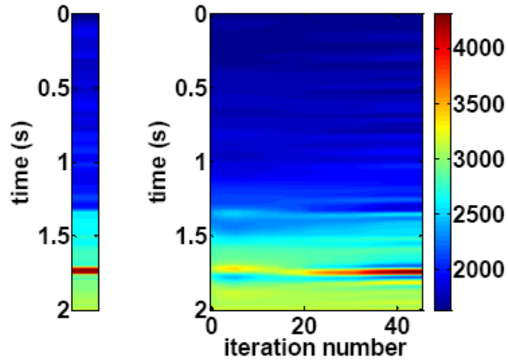

(a) (b)

FIG. 8: FWI inversion updates at 1800m lateral position. a) The true velocity b) Velocity profiles updates vs. Iteration numbers.

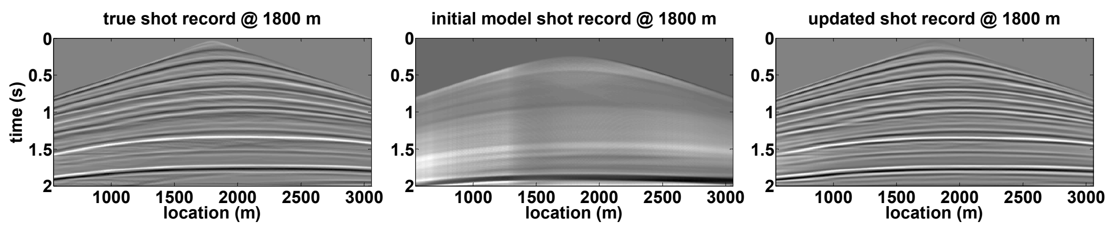

(a) (b) (c)

FIG. 9: FWI inversion shot prediction at 1800*m* lateral position (with 0.2*s* AGC window and minimum phase wavelet with 12 Hz dominant frequency). a) The true shot record b) the initial shot record c) the updated shot record after 45 iterations.

CONCLUSION

The main conclusion of this work is that the linearized solution of seismic reflection inverse problem can be obtained using the fast PSTM and corresponding forward modeling. It requires updating the velocity in time and it incorporates accurate diffraction stack weighting of the PSTM data. The result of the method will be an updated velocity in time that can be used in time to depth conversion. The accuracy of this approach is higher in the mediums with smaller lateral velocity variations.

We used Equivalent Offset Migration (EOM) that is based on Kirchhoff PSTM. The advantage of using EOM is the starting velocity in update procedures that are obtained from the Common Scatter Point (CSP) gathers. As an example the method is tested on Marmousi velocity model.

ACKNOWLEDGMENTS

We thank the sponsors, faculty, staff and students of CREWES and the Natural Sciences and Engineering Research Council of Canada (NSERC) for their support of this work. We also would like to thank Abdolnaser Yousefzadeh, Dr. Kristopher Inannen, Marcus Wilson and Ben Wards for their useful comments and suggestions.

REFERENCE

Bancroft, J. C., Geiger, H. D., and Margrave, G. F., 1998, The equivalent offset method of prestack time migration: Geophysics, **63**, 2042-2053.

Bleistein, N., J. K. Cohen, and J. W. S. Jr., 2001, Mathematics of multidimensional seismic imaging, migration, and inversion: Springer Verlag.

Cohen, J, .K. and Bleistein, N,. 1979, Velocity inversion procedure of acoustic waves: Geophysics, **44**, 1077-1087.

Innanen,K., 2011, Geophysical inversion II: seismic inversion:U of Calgary, unpublished course notes.

Ma, Y., 2010, Full waveform inversion with image-guided gradient: Master of Science Thesis , Center for Wave Phenomena, Colorado School of Mines

Margrave, G. F,. Ferguson R. J., and Hogan C. M., 2010, Full waveform inversion with wave equation migration and well control: CREWES Annual Research Report.

Pratt, R. G., 1990, Inverse theory applied to multi-source cross-hole tomography. Part II: Elastic wave-equation method: Geophysical Prospecting, **38**, 311–330.

Pratt, R. G., 1999, Seismic waveform inversion in the frequency domain, Part I: Theory and verification in a physical scale model: Geophysics, **64**, 888-901.

Pratt, R. G., C. Shin, and G. J. Hicks, 1998, Gauss-Newton and full Newton methods in frequency-space seismic waveform inversion: Geophysical Journal International, **133**, 341–362.

Schneider, W. A., 1978, Integral formulation for migration in two and three dimensions: Geophysics, **43**, 49-76.

Sirgue, L., and Pratt, R. G., 2004, Efficient waveform inversion and imaging: A strategy for selecting temporal frequencies: Geophysics, **69**, NO. 1, 231.

Sun, J., and Gajewski, D., 1997, True-amplitude common-shot migration revisited: Geophysics, 62, 1250–1259.

Symes, W. W., 2008, Migration velocity analysis and waveform inversion: Geophysical Prospecting, **56**, NO. 6, 765–790.

Tarantola, A., 1984, Linearized inversion of seismic reflection data: Geophysical Prospecting, **32**, 998-1015.

Virieux, J., and S. Operto, 2009, An overview of full-waveform inversion in exploration geophysics: Geophysics, **74**, WCC127-WCC152

Vigh, D., and Starr, W., 2008, 3D prestack plane-wave, full-waveform inversion: Geophysics, **73**, VE135–VE144

.